Temperature and size dependence of electron magnetic resonance spectra of Ni nanoparticles embedded in an amorphous SiO_2 matrix

2009 J. Phys.: Condens. Matter 21 456001

(http://iopscience.iop.org/0953-8984/21/45/456001)

J. Phys.: Condens. Matter **21** (2009) 456001 (9pp) doi:10.1088/0953-8984/21/45/456001

Temperature and size dependence of electron magnetic resonance spectra of Ni nanoparticles embedded in an amorphous SiO_2 matrix

V Singh and M S Seehra[1]

Department of Physics, West Virginia University, Morgantown, WV 26506-6315, USA

E-mail: mseehra@wvu.edu

Received 5 August 2009, in final form 25 September 2009
Published 21 October 2009
Online at stacks.iop.org/JPhysCM/21/456001

Abstract

Investigations of spin dynamics in Ni nanoparticles (NPs) with diameters $D = 3.8$, 11.7, 15 and 21 nm embedded in an amorphous SiO_2 matrix of composition 15/85 (Ni/SiO_2) are reported using EMR (electron magnetic resonance) spectroscopy at 9.28 GHz. Three resonance lines are observed whose EMR parameters, namely linewidth ΔH, resonance field H_r and intensity I_o, are measured from 5 to 300 K. Line 1 with temperature-independent $\Delta H = 50$ Oe and $g \approx 2$, and intensity varying as $1/T$, is shown to result from paramagnetic defects in the SiO_2 matrix. Lines 2 and 3, with $g \approx 2.2$ and 8, respectively, and temperature-dependent EMR parameters are assigned to Ni NPs. While line 2 with $g \approx 2.2$ is due to the majority of Ni NPs, the source of line 3 is discussed in terms of two possibilities: (i) large clusters of blocked Ni NPs and (ii) the inherent part of the composite asymmetric line made up of lines 2 and 3 predicted by the Raikher–Stepanov (RS) model for dispersed ferromagnets. The temperature dependence of ΔH (full width at half-maximum) of the composite line obtained by integration of the EMR spectra decreases with the increase in temperature, reaching a minimum near 300 K in agreement with the RS model. The observed decreasing asymmetry of the composite absorption spectra with increasing temperature is also in agreement with the predictions of the RS model, thus providing a satisfactory explanation for the observed temperature dependence of the EMR spectra of Ni NPs. Large clusters of blocked Ni NPs as the source of line 3 are ruled out and additional tests for the RS model are proposed. The decreasing magnetization with decreasing particle size of Ni NPs observed here is discussed in terms of the possible roles of the surface disordered spins and Ni–SiO_2 interaction.

1. Introduction

A current area of intense research activity is how the properties of magnetic nanoparticles (NPs) vary with the change in the size of NPs from about 100 nm to a few nm. This interest is driven in part by the size-dependent properties of NPs and partly by their potential applications in biomedicine [1, 2], catalysis [3] and sensors [4]. In addition to measurements of change in magnetization M with variations in temperature T and magnetic field H, ac susceptibility measurements are often used to determine the relaxation parameters. Electron magnetic resonance (EMR) spectroscopy is a complementary technique since it provides details of spin dynamics and magnetic interactions not available from other techniques.

Bulk Ni is a classic metallic ferromagnet with Curie temperature $T_C = 631$ K. There have been a number of studies on NPs of Ni partly because of their application in catalysis [3, 5, 6]. Reported works include magnetic susceptibility studies of Gittleman *et al* on Ni granular films sputtered on SiO_2 and Al_2O_3 substrates [7], magnetic studies of Sahoo *et al* on 5 nm particles [8], magnetic studies of Zhang *et al* on 10 nm particles [9], and magnetic and ac susceptibility studies of Goya *et al* on the 3 nm Ni/SiO_2 system [10].

In none of the above reported studies were systematic investigations of the changes in the magnetic properties with

[1] Author to whom any correspondence should be addressed.

the change in the size of the Ni NPs carried out. Recently we undertook such investigations on the Ni NPs embedded in an SiO_2 matrix with the nominal composition Ni/SiO_2 (15/85) and reported changes in the blocking temperature of the 3.8 nm NPs with applied magnetic field and measuring frequency [11]. In a subsequent paper, relaxation parameters using ac susceptibility measurements for NPs of Ni in the Ni/SiO_2 nanocomposite with diameters $D = 3.8$, 11.7, 15 and 21 nm for the Ni NPs were presented [12]. In this paper, we report results on the changes in the temperature dependence of the EMR spectra measured at 9.28 GHz for the same samples with $D = 3.8$, 11.7, 15 and 21 nm, along with their measured magnetizations up to 65 kOe. In the EMR spectra, three resonance lines are observed, two of which are assigned to Ni NPs and the third narrower line near $g = 2.0$ is shown to be due to paramagnetic defects in the supporting amorphous SiO_2 matrix. The temperature dependence of the resonance field H_r, linewidth ΔH, and intensity I_o for all three lines are investigated for the 5–300 K range. These results of H_r, ΔH and I_o for the two lines due to Ni are interpreted in terms of the size and temperature dependence of the magnetic anisotropy of these particles in the polycrystalline dispersed system. The asymmetry and the inhomogeneous broadening of the composite absorption line due to the Ni NPs (caused by scattering in orientation of the anisotropy axis) is progressively suppressed in the superparamagnetic region with increasing temperatures. The saturation magnetization also decreases with the decrease in the size of the NPs. Details of these results along with their interpretation and discussions are presented below.

2. Experimental details

The samples of Ni/SiO_2 (15/85) nanocomposites were synthesized by the sol–gel route using $Ni(NO_3)_2{\cdot}6H_2O$, TEOS (tetraethylorthosilicate), anhydrous citric acid, anhydrous ethylene glycol and ethanol [3, 10]. Briefly, $Ni(NO_3)_2{\cdot}6H_2O$ and TEOS in appropriate amounts are added to a solution of citric acid in alcohol and homogenized at room temperature for 15 min. This is followed by adding ethylene glycol and polymerizing the solution for several hours at 80 °C, resulting in a solid resin. The solid resin is then heated in air at 300 °C for 6 h. The resulting compound is thoroughly ground by mortar and pestle and then annealed at selected temperatures between 400 and 800 °C in flowing UHP (ultrahigh pure) N_2 gas for 2 h to obtain particle sizes of Ni in the range of 3.8–23 nm. If ordinary grade N_2 is used, then some NiO was always detected in the x-ray diffraction (XRD) patterns.

The XRD patterns of the samples annealed at 400, 500, 600, 700 and 800 °C, using a Cu Kα source with $\lambda = 1.541\,85$ Å, are shown in figure 1. Except for the broad line centered near $2\theta = 24°$ due to the amorphous SiO_2 matrix, all the remaining lines are due to FCC Ni. The diameters D of the particles were determined from the width of the lines as well as from transmission electron microscopy (TEM) of the particles. In our other publications [11–13] TEM micrographs and resulting size distribution for various sizes were shown.

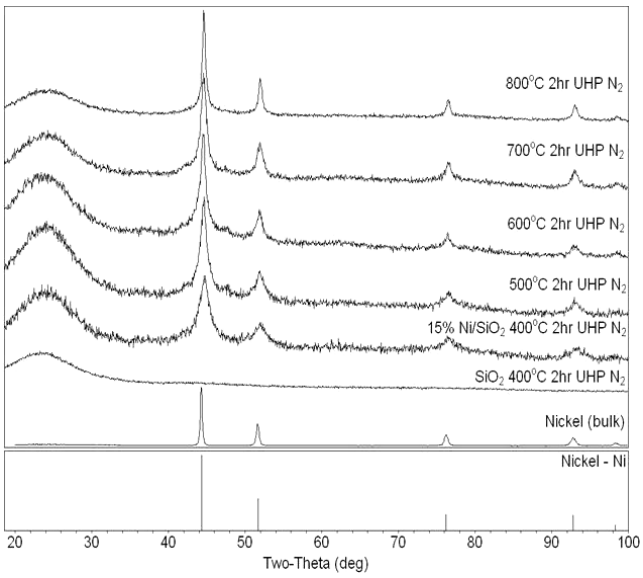

Figure 1. Room temperature XRD patterns of the Ni/SiO_2 samples annealed at various temperatures in ultrahigh pure (UHP) N_2 gas. For comparison, XRD of bulk Ni and expected line positions for FCC Ni are also shown.

Analysis of TEM micrographs for all five sizes yielded log-normal size distributions with mean $D = 3.8$, 11.7, 15, 21 and 23 nm and standard deviation $\sigma \approx 0.2$ for samples annealed at 400, 500, 600, 700 and 800 °C, respectively. Sizes determined from the Williamson–Hall analysis of the XRD data were consistent with the results from TEM [13]. Two additional samples were prepared without any Ni doping by annealing them at 400 and 800 °C to determine the nature of any background EMR signal from SiO_2.

The EMR spectra at 9.28 GHz were recorded using a conventional reflection type x-band (9.28 GHz) spectrometer in conjunction with a variable-temperature cryostat (Oxford Instruments) to yield the spectra in the temperature range of 5–300 K. As usual, the recorded signals represent the first derivative of the absorption curve with respect to sweeping field H and the reported linewidths are peak-to-peak separations in the absorption derivatives. Integration of the EMR spectra to yield absorption profiles at different temperatures is also presented. Magnetizations were measured with a commercial SQUID magnetometer.

3. Experimental results

A comparison of the EMR first-derivative signals observed at 5 K in the five samples of different sizes is shown in figure 2. Three EMR lines are observed: (i) the narrow line 1 near $g = 2.00$ whose intensity decreases with increase in particle size; (ii) the broad line 2 centered near $g = 2.25$ whose signature does not appear to change with changes in particle size and (iii) absorption marked 3 at the lower fields for which only a part of the line is observed even at 5 K. The profiles of the observed EMR spectra at different temperatures from 5 K to room temperatures for two representative samples, namely samples with sizes $D = 3.8$ and 21 nm, are shown in figures 3

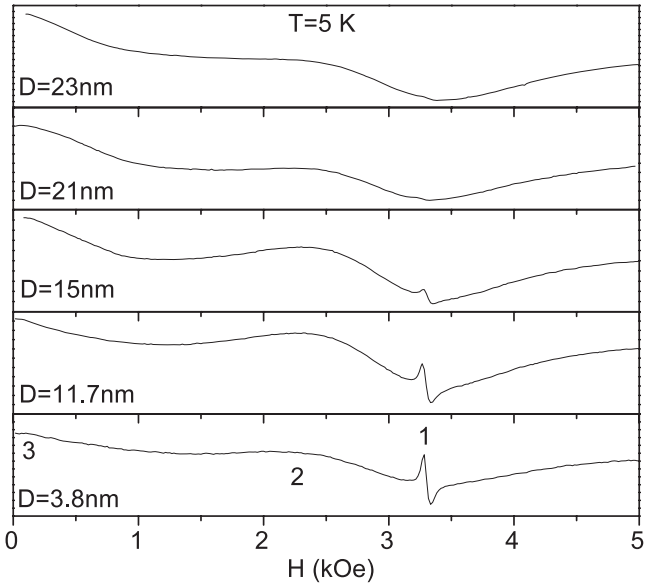

Figure 2. EMR absorption derivative profiles of the various Ni/SiO_2 samples with sizes from 3.8 to 23 nm measured at 5 K. The numbers 1, 2 and 3 label the three lines discussed in the text.

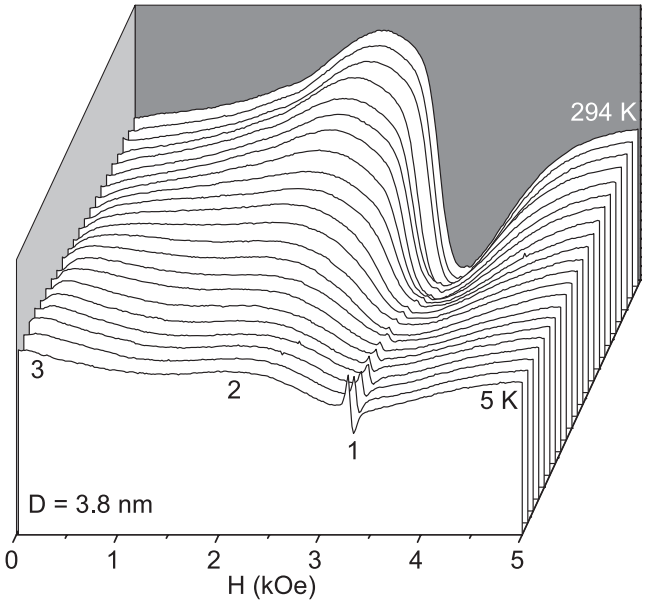

Figure 3. Recorded EMR line profiles for the 3.8 nm particles at $T = 5$, 10, 16, 20, 31, 40, 54, 68, 83, 93, 107, 121, 133, 150, 170, 190, 204, 217, 240, 260, 280 and 294 K.

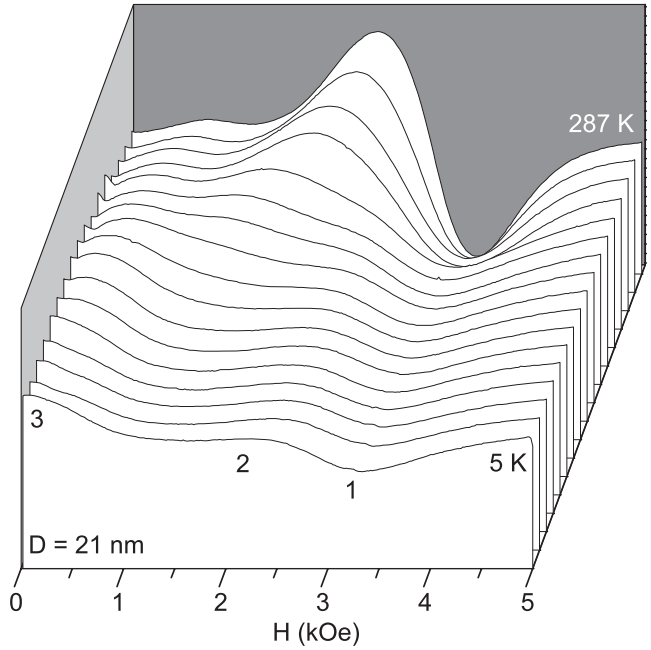

Figure 4. Recorded EMR line profiles for the 21 nm particles at $T = 5$, 13, 18, 28, 45, 58, 70, 85, 95, 110, 122, 132, 147, 170, 190, 230 and 287 K.

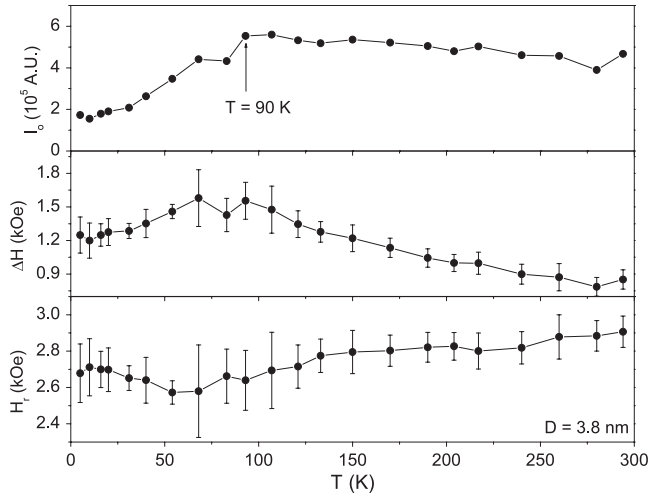

Figure 5. Temperature variations of the intensity I_o, linewidth ΔH and resonance field H_r of line 2 in 3.8 m particles are shown. The lines connecting the data points are for visual aid.

and 4, respectively. All the profiles in figures 3 and 4 were recorded using the same spectrometer parameters such as gain. Results for other samples are similar [13]. It is evident that the intensity of line 1 decreases with increase in temperature and with increase in particle size. For line 3, profiles shift to higher fields with increase in temperature, although the line is not well resolved. Therefore it is difficult to accurately measure its resonance field H_r and linewidth ΔH.

For the two representative samples with sizes $D = 3.8$ nm and 21 nm, the temperature dependence of H_r, ΔH and the line intensity I_o of line 2 are plotted in figures 5 and 6, respectively. The relation $I_o = \alpha(\Delta H)^2 L$ is used for calculations of I_o, where L is the peak-to-peak height of the absorption derivative and $\alpha = 3.63$ for a Lorentzian line. It is evident that the intensity I_o and linewidth ΔH peak at a certain temperature which we associate with the blocking temperature T_B(EMR) = 90 K and 122 K for the $D = 3.8$ nm and $D = 21$ nm samples, respectively, followed by decreasing magnitudes of these quantities with decreasing T for $T < T_B$. The line positions H_r appear to have a minimum at T_B so that the lineshifts $H_r(300\text{ K}) - H_r(T)$ will also peak at $T = T_B$ (EMR). These magnitudes of T_B (EMR) measured at 9.28 GHz are higher

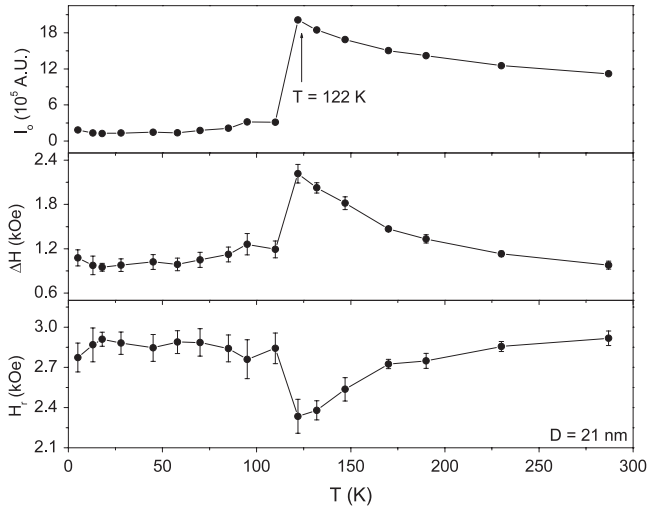

Figure 6. The same as in figure 5 except for the $D = 21$ nm sample.

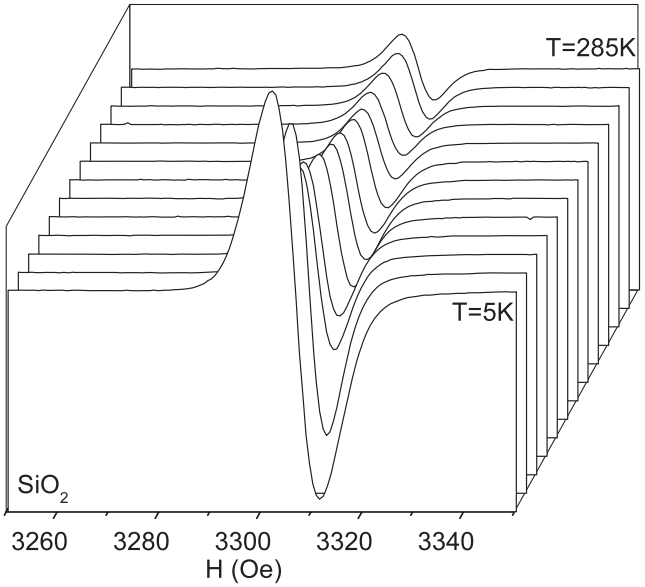

Figure 7. Line profiles of EMR spectra in the undoped SiO_2 sample annealed at 400 °C. The line profiles shown are for temperatures $T = 5$, 20, 40, 56, 70, 83, 100, 120, 155, 195, 235, 265 and 285 K.

than those measured at ac frequencies <1 kHz due to the measuring frequency dependence of T_B and the effect of the applied resonance field H_r [11–13]. An interpretation of the temperature variations of figures 5 and 6 is given later in this paper. Similar variations were observed for the other sizes [13].

For the sample of SiO_2 prepared similarly but without any Ni doping and annealed at 400 °C, a narrow line of width $\Delta H = 9$ Oe and $g = 2.00$ is observed. The EMR line profiles for this line at different temperatures are shown in figure 7 and the temperature dependence of its EMR parameters is shown in figure 8. The line intensity I_o varies nearly as $1/T$ with ΔH and H_r being essentially temperature-independent. For comparison, the temperature dependence of the EMR line 1 observed in the $D = 3.8$ nm of Ni/SiO_2 has a similar variation (figure 8).

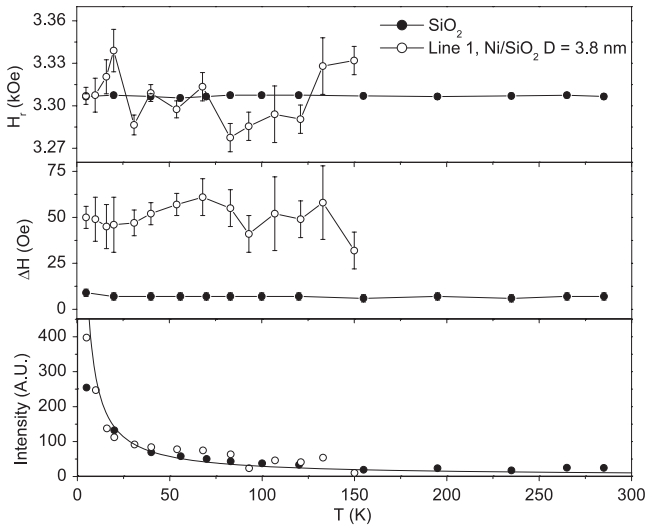

Figure 8. Temperature variations of the EMR parameters for line 1 in the undoped SiO_2 annealed at 400 °C and in the 3.8 nm Ni/SiO_2 sample. The solid line in the bottom figure for intensity is a $1/T$ variation. For the variation of H_r and ΔH, lines connecting the data points are for a visual aid.

4. Interpretation of line 1

As mentioned earlier, the narrow EMR line 1 (figures 2, 7 and 8) is attributed to paramagnetic defects in the SiO_2 matrix for the following reasons: first, the measured g value of 2.00 for line 1 is different from $g \approx 2.25$ measured and expected from Ni; and second, its temperature-independent ΔH and H_r and $1/T$ dependence of intensity is characteristic of paramagnetism. In a number of earlier studies of NPs of iron oxides, the observed narrow line has been attributed to superparamagnetic small nanoparticles present in the samples [14–17]. However, in those cases, the $g = 2.00$ of the narrow line was identical to that of the main line attributed to most of the other particles. In addition, as discussed later, ΔH and H_r for a superparamagnetic resonance are expected to be temperature-dependent, in contrast to the observations of temperature independence of these parameters for line 1 in figure 8.

Another observation regarding line 1 in our samples is that the intensity of this line weakens as the size of the Ni NPs increases (see figures 2–4). As noted earlier (figure 1), the annealing temperature determines the size of the Ni NPs in that higher annealing temperature yields particles of larger D. To verify whether a higher annealing temperature might be quenching the paramagnetic defects responsible for line 1 in the larger sizes of the Ni NPs, a sample of undoped SiO_2 annealed at 800 °C was also prepared. In figure 9, the EMR signals observed from samples of SiO_2 annealed at 400 and 800 °C are compared. Indeed, the EMR signal observed in the 800 °C annealed sample is nearly two orders of magnitude weaker, thus explaining our observations of the size dependence of the intensity of line 1 in the Ni/SiO_2 samples.

Although the temperature dependence of the EMR of line 1 in the 3.8 nm Ni/SiO_2 and undoped SiO_2 is similar (figure 8), the magnitude of ΔH for line 1 in the 3.8 nm sample of

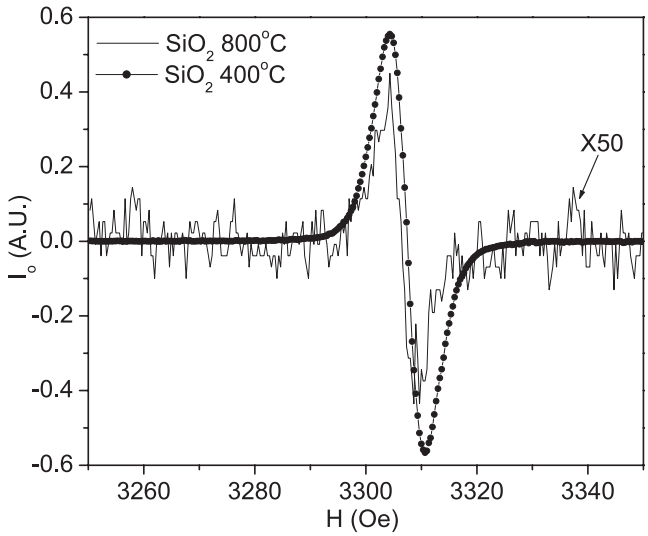

Figure 9. Comparison of the line profiles of line 1 measured at 300 K for the undoped samples of SiO_2 annealed at 400 and 800 °C.

Ni/SiO_2 is larger ($\Delta H \approx 50$ Oe) than $\Delta H \approx 9$ Oe for the line observed in the undoped SiO_2. This larger ΔH for line 1 in Ni/SiO_2 is likely due to the effect of dipole interaction on the paramagnetic defects from the neighboring Ni nanoparticles. In this study, the nature of the paramagnetic defects responsible for line 1 was not explored since there is considerable literature on the various EMR active paramagnetic defects in amorphous silica [18] and the nature of the defect is not relevant to the main subject of this paper, namely the EMR spectra due to Ni NPs.

5. Theoretical considerations for lines 2 and 3

Prior to the interpretation of the EMR parameters for lines 2 and 3, it is useful to summarize the results from relevant theoretical models and the known relevant properties of bulk Ni. FCC Ni (density = 8.91 g cm^{-3}, lattice constant = 3.52 Å) is a ferromagnet with T_C = 631 K, ⟨111⟩ directions as the easy axes and saturation magnetization M_S = 510(485) emu cm^{-3} near 0 K (293 K). The first-order anisotropy constant K_1 is negative with magnitudes = $7.5 \times 10^5 (5 \times 10^4)$ ergs cm^{-3} at 20 K (293 K) [19]. The above magnitudes yield the effective anisotropy field $H_A = -(2K_1/M_S)$ = 1470 Oe (103 Oe) near 20 K (293 K). The negative sign of anisotropy constant K_1 merely reflects the fact that, in bulk Ni, ⟨111⟩ is the easy direction of magnetization rather than the ⟨100⟩ direction.

In the earlier EMR studies of polycrystalline bulk ferromagnets, the resonance field was successfully fitted to the equation $H_r = (\omega/\gamma) - H_i$, where H_i is an effective internal field, $\omega = 2\pi f_m$ and $\gamma = 2\pi g \mu_B / h$ [20]. For the magnetocrystalline anisotropy of cubic systems, $H_i = -2K_1/M_S = H_A$. For bulk Ni, K_1 is negative and so H_A is positive, leading to a shift of the line to lower fields. If $H < H_A$, two lines are often present. The lower (higher) field peak belongs to grains with magnetization parallel to the easy axis (the applied field).

The above results suitable for bulk Ni cannot be directly applied to EMR in Ni NPs first because magnitudes of K_1 are larger for the smaller particles [12] and second because H_A is reduced with increasing temperatures due to the effect of superparamagnetism [6, 21]. Raikher and Stepanov (RS) have presented a model on the effect of thermal fluctuations on the FMR lineshapes in dispersed ferromagnetic nanoparticle systems for the uniaxial and cubic ($K_1 < 0$ and $K_1 > 0$) symmetries [22]. Therefore the RS model is a relevant one for comparison with our experimental results in the Ni NPs.

As noted by RS [22], the calculations require 'averaging not only over the statistical ensemble of particles with a given direction of the anisotropy axis, but also over the angular distribution of the anisotropy axis in such a particle.' In [21], only the first averaging was carried out. Since this analysis of [21] provides considerable insight into the size and temperature dependence of the anisotropy, we apply it to our Ni NPs to show how temperature and size dependence of H_A^{SP} (superparamagnetic) relative to bulk H_A changes with temperature due to the effect of superparamagnetism of Ni NPs. The more complete analysis of the RS model makes the following major predictions which are tested, at least qualitatively, in this work on the Ni NPs:

(i) With decreasing temperature, the EMR absorption becomes increasingly asymmetric, resulting in the appearance of two lines in the experimental absorption derivative. The separation between the two lines in the absorption derivative increases with the decrease in temperature.

(ii) Beginning at the lowest temperature, the linewidth ΔH decreases with increase in temperature (irrespective of the type or the sign of anisotropy constant), reaches a minimum at a certain temperature and then, at high enough temperatures, ΔH of the now symmetric line is predicted to increase with increase in temperature.

(iii) The resonance field H_r, defined by the zero of the absorption derivative of the higher field line, is predicted to decrease with decreasing temperatures for cubic systems with $K_1 < 0$ but increase for systems with $K_1 > 0$.

The effect of averaging over the angle θ between the magnetic moment and the magnetic field, done in [21], leads to the following ratio of H_A^{SP}/H_A (bulk) for cubic anisotropy:

$$H_A^{SP}/H_A = \frac{1 - 10x^{-1}\coth(x) + 45x^{-2} - 105x^{-3}\coth(x) + 105x^{-4}}{\coth(x) - x^{-1}}. \quad (1)$$

Here H_A is the anisotropy field for bulk Ni and $x = M_S V H / kT$ with V being the volume of the nanoparticle with intrinsic moment M_S and k the Boltzmann constant. In figure 10, the computed plots of H_A^{SP}/H_A versus T are shown for the different sizes of NPs investigated in this work using H = 2800 Oe, the field close to H_r for line 2. These plots are valid for the superparamagnetic regime only, namely $T > T_B$ (EMR). It is evident from figure 10 that, with the decrease in temperature, H_A^{SP} increases for all the particles. Of course in

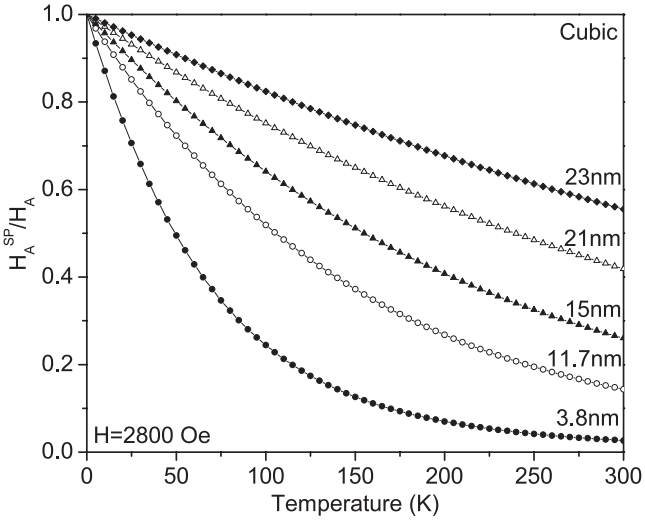

Figure 10. Plots of H_A^{SP}/H_A for the sizes of Ni NPs shown versus temperature using equation (1). Magnitude of $H = 2800$ Oe close to H_r for line 2 is used in the calculations.

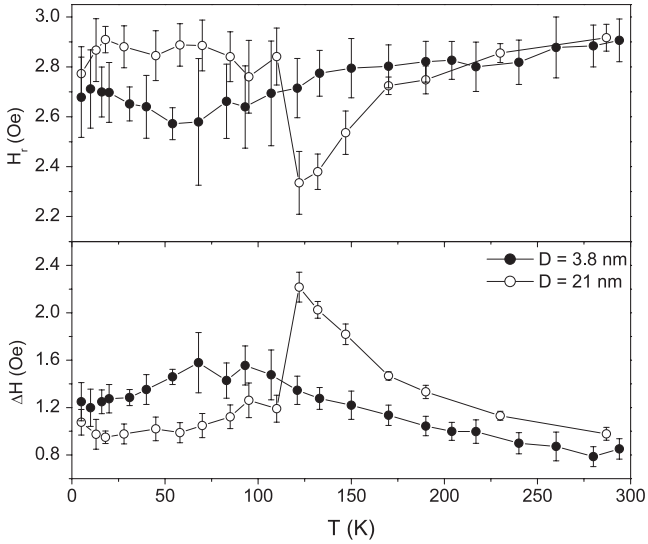

Figure 11. Comparison of the temperature dependence of H_r and ΔH for line 2 in the 3.8 and 21 nm samples of Ni/SiO_2. Lines joining the points are for a visual aid.

our case, T_B (EMR) $>$ 90 K for all the particles and data for temperatures above T_B only can be compared with the predictions of equation (1).

6. Interpretation of lines 2 and 3

In the earlier EMR work of Sharma and Baiker in the Ni/SiO_2 system [6], a weaker absorption at lower fields and lower temperatures only, somewhat similar to line 3 reported here, was observed in addition to the main line near $g = 2.25$. This lower field absorption was suggested to result from the larger blocked particles in the ferromagnetic state. The more intense line near $g = 2.25$ is then from the majority of the Ni NPs which go through the superparamagnetism to ferromagnetic state as the temperature is lowered. In this interpretation, lines 2 and 3 are treated as distinct entities. Since this may be a reasonable interpretation, although different from the RS model, it is first followed in the interpretation of the data below. A comparison and critique of these two models is given later.

The temperature dependence of the EMR parameters for the two representative samples with $D = 3.8$ nm and 21 nm were given earlier in figures 5 and 6, respectively. A common feature of the data in figures 5 and 6 and for the remaining samples with different sizes [13] is that, with the decrease in temperature from 300 K, the intensity I_o, linewidth ΔH and lineshift $\delta H_r = H_r(300\text{ K}) - H_r(T)$ for line 2 increase with the decrease in T, reaching maximum values at a certain temperature T_B (EMR). For $T < T_B$ (EMR), I_o and ΔH decrease with decrease in T whereas H_r is nearly temperature-independent within experimental uncertainties. We associate T_B (EMR) with the blocking temperature measured at 9.28 GHz and at the resonance field H_r. For $T > T_B$ (EMR), the particles are in the superparamagnetic state whereas for $T < T_B$ (EMR), the Ni spins appear blocked at the 9.28 GHz frequency, resembling ferromagnetism.

For the 3.8 nm sample, a detailed investigation of the variation of T_B measured at $f_m = 1$ Hz and in different magnetic fields H yielded the variation $T_B(H) = 33(1 - H/H_o)^m$ with $H_o = 3200$ Oe and $m = 2(3/2)$ for lower (higher) fields, in agreement with theoretical predictions [11]. This rapid decrease of T_B with increasing H implies that T_B (EMR) measured in H_r should be considerably lower than the theoretical estimate calculated for $f_m = 9.28$ GHz in zero H based on the equation $T_B = T_o + T_a/\ln(f_o/f_m)$. Here T_o represents the interparticle interaction, $T_a = K_a V/k_B$ and $f_o = 1.8 \times 10^{10}$ Hz for the Ni/SiO_2 system [12]. Using the data of [12] for $T_o = 0$, 0, 6.6 and 12.5 K and $T_a = 310$, 954, 1334 and 1405 K yields T_B(EMR) = 460, 1416, 1987 and 2098 K for $H_r = 0$, respectively, for the $D = 3.8$, 11.7, 15 and 21 nm samples. To determine the effect of the applied field H_r on T_B (EMR), we use the theoretical fit of $T_B(H)/T_B(0)$ versus H from [11], which gives $T_B(H)/T_B(0) \approx 0.08$ at $H = H_r$. This yields T_B (EMR) at $H = H_r$ equal to 37, 113, 160 and 168 K, which compares favorably with the experimental T_B (EMR) = 90, 115, 155 and 122 K, respectively for the $D = 3.8$, 11.7, 15 and 21 nm samples. Thus the measured values of T_B (EMR) can be explained satisfactorily once the magnetic field dependence of T_B (EMR) is taken into account.

The decrease of H_A^{SP} with increasing temperatures for all sizes due to increasing thermal fluctuations in figure 10 can be used to qualitatively explain the temperature dependence of ΔH and H_r for $T > T_B$ (EMR). Since H_A and hence H_A^{SP} are both positive for Ni, the line shifts to lower fields following our earlier discussion in section 5. Also, since anisotropy increases with decreasing temperatures in figure 10, H_r is predicted to decrease with decreasing temperature as observed experimentally. Furthermore, anisotropy also increases the linewidth ΔH if the anisotropy does not commute with the magnetization M_Z measured along the direction of applied field H_r [20, 23, 24]. Therefore ΔH should also increase with decreasing temperatures. These effects of decreasing H_r and

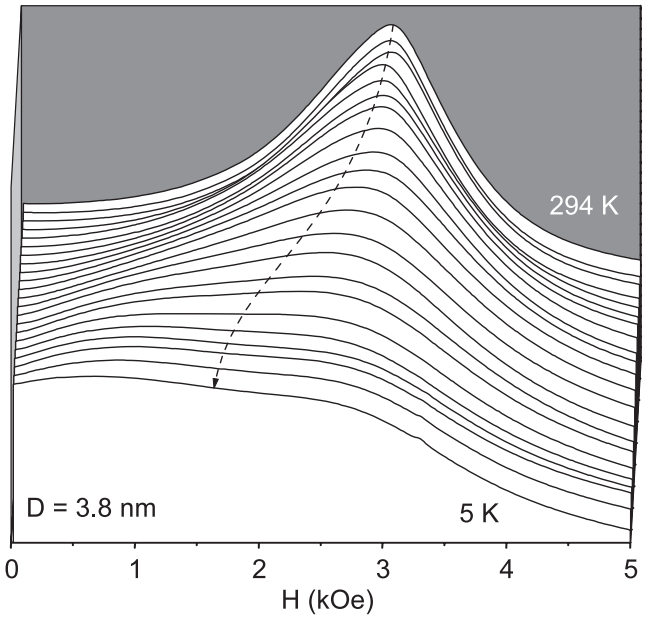

Figure 12. EMR absorption spectra obtained by integration of the experimental derivative spectra of figure 3 for $D = 3.8$ nm NPs. The dotted line is drawn connecting the center of the composite spectra.

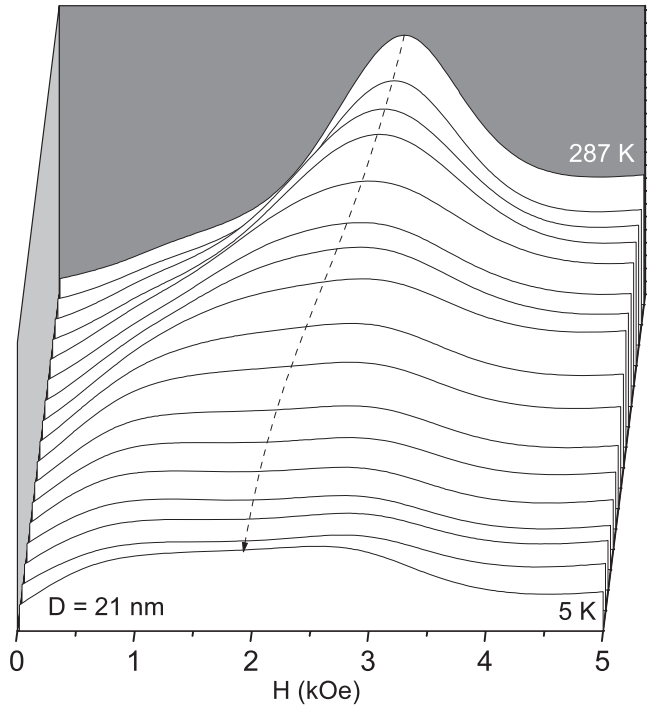

Figure 13. Absorption spectra for the $D = 21$ nm NPs obtained by integration of the experimental derivative EMR spectra of figure 4. The dotted line is drawn connecting the center of the composite two-line spectra

increasing ΔH on lowering the temperature are observed here for NPs of Ni (figures 5 and 6). For the two representative sizes of $D = 3.8$ and 21 nm, the temperature dependences of ΔH and H_r shown in figure 11 are consistent with this prediction. Also the larger magnitude of ΔH in the 21 nm vis-à-vis 3.8 nm is consistent with the predicted higher anisotropy of the 21 nm particles (figure 10). Although these magnitudes of ΔH are comparable to $H_A = 1470$ Oe calculated earlier for bulk Ni at lower temperatures, the anisotropy in Ni NPs is affected by several other factors noted above.

To determine whether demagnetizing effects due to any deviations from spherical symmetry of the Ni NPs might be affecting our observations, we measured EMR of a polycrystalline Ni thin foil of thickness 0.01 mm at room temperature. For in-plane EMR at 9.28 GHz, we measured $H_r \approx 1300$ Oe with $\Delta H \approx 1600$ Oe where, for $H \perp$ plane, $H_r \approx 8500$ Oe with a highly asymmetric line. Assuming $M_s = 485$ emu cm^{-3} for bulk Ni at 293 K and demagnetizing factors of $N_\parallel = 0$ and $N_\perp = 4\pi$, the Kittel equations yield $H_r(\parallel) \approx 1240$ Oe for in-plane and $H_r(\perp) \approx 9108$ Oe resonance fields [25]. The slight deviations of the experimental values from the above magnitudes are most likely due to the finite thickness of the foil, leading to $N_\parallel > 0$ and $N_\perp < 4\pi$. For the thin film, shape is the leading source of anisotropy, yielding departures from the expected $g = 2.25$ for Ni. In the Ni NPs, we observe $g \approx 2.25$ for all of our samples at room temperature suggesting negligible effects of any shape anisotropy on the EMR spectra. These results also show that $H_r \approx 700$ Oe for line 3 in figures 12 and 13 cannot be explained just in terms of the shifts due to demagnetizing effects in a ferromagnetic particle since $H_r \approx 1240$ Oe for in-plane resonance in a thin film, which provides the maximum possible shift due to a demagnetization factor, is larger than 700 Oe. In addition, line 3 is observed even in the smallest 3.8 nm particle which is unlikely to have any large clusters of Ni NPs. For these reasons, large blocked particles as the source of line 3 can be ruled out.

Next, our experimental results are compared with some of the predictions of the RS model. For this comparison, we have integrated the spectra of figures 3 and 4 to yield absorption curves of figures 12 and 13 for the 3.8 nm and 21 nm systems, respectively. According to the RS model, line 3 appears as a result of the averaging over the angular distribution of the anisotropy axis in NPs and so it is an integral part of line 2 which results in an asymmetric lineshape as temperature is lowered. This is clearly observed in figures 12 and 13. The temperature dependence of the resonance field H_r shown in figures 5, 6 and 11 is still valid since H_r in the RS model is determined by the field position of zero intensity in the derivative spectra of line 2. In figures 12 and 13, the dotted lines are drawn connecting the center of the composite absorption spectra which also shifts to lower magnetic fields with decreasing temperatures. In the RS model, linewidth is defined as the field separation between the minimum of line 2 and the maximum of line 3 in the absorption derivative. This separation in figures 3 and 4 does decrease with the increase in temperature. However, the peak of line 3 is difficult to define at many temperatures. Therefore, for the linewidth of the composite line, we measured FWHM (full width at half-maxima) of the absorption spectra in figures 12 and 13. The temperature dependence of the FWHM linewidth so measured is shown in figure 14 for the 3.8 and 21 nm particles. The decrease in the linewidth with increasing temperatures

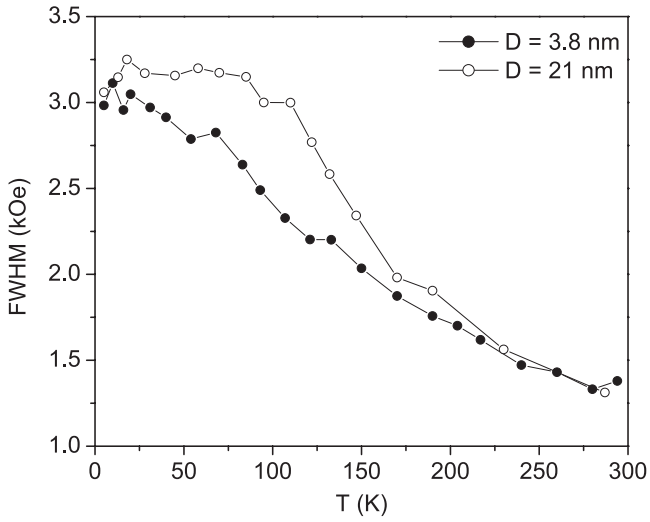

Figure 14. Temperature dependence of the linewidth FWHM (full width at half-maxima) of the composite line for the $D = 3.8$ and 21 nm NPs. Lines joining the points are for a visual aid.

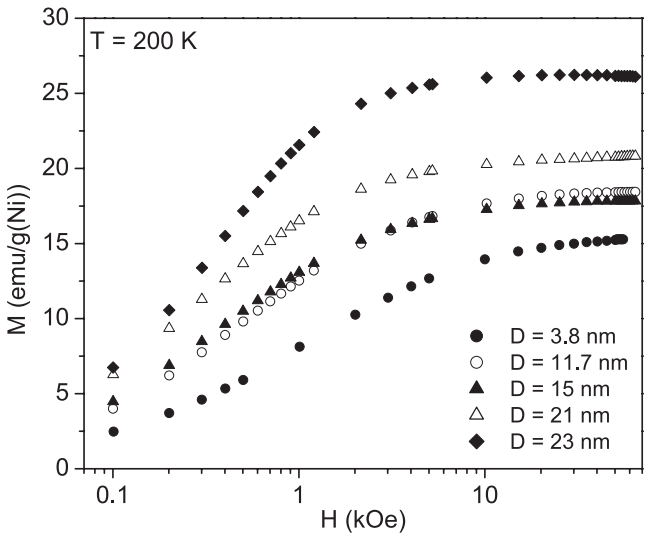

Figure 15. Variations of static magnetization M with applied field H at 200 K for the particle sizes shown.

predicted in the RS model is clearly observed with a clear minimum near 300 K, at least for the smaller 3.8 nm particles. This result, along with the decreasing asymmetry with increasing temperatures and temperature dependence of H_r, is in agreement with the predictions of the RS model for a cubic system with negative K_1 as noted earlier. Experiments at still higher temperatures are needed to determine the predicted increase in linewidth for $T > 300$ K.

There have been a number of other nanoparticle systems where similarly increasing ΔH and lineshifts δH_r with decreasing temperatures have been reported [26–31]. Nagata and Ishihara [26] while considering the case of shape anisotropy due to an ellipsoidal particle showed that lineshift (δH_r) is proportional to $(\Delta H)^n$, where $n = 3$ for randomly oriented particles and $n = 2$ for partially oriented particles. For NPs of NiO [31], Mn–Zn ferrite [26], ferrihydrite [28] and Si-doped ferrihydrite [29], $n = 3$ has been experimentally observed. However, these systems have dominant antiferromagnetic coupling and the EMR is due to uncompensated magnetic moments on the surface of the NPs. Therefore, results from these systems cannot be compared with our results in Ni NPs, bulk Ni being a ferromagnet.

An alternative approach to the line narrowing observed in NPs with increasing temperature was developed by Morais *et al* [32, 33] using the van Vleck moment method. For isolated NPs interacting only by long-range dipole interaction, this model predicted ΔH varying as $\tanh(\Delta E/2kT)$, with ΔE being an activation energy whereas for an interacting spin system including exchange and dipole interactions, this model predicts ΔH varying as $\exp(-T/T_f)$. Both of these variations predict decreasing ΔH with increasing T but $\exp(-T/T_f)$ represents a more rapid variation [33]. These models, however, did not address the question of changes in H_r with changing temperature which has been observed here as well as in many systems of NPs [26–31]. Therefore, this model is not used here to analyze the experimental results on the Ni NPs.

Finally in figure 15, the plots of M versus H at 200 K for all five samples of Ni NPs show a decrease in the saturation magnetization M_s with decrease in particle size, similar to the recent observations in Fe_3O_4 NPs [34]. Similar variation with D is observed at 5 K [13]. In figure 15, the maximum magnitude of $M_s = 27$ emu g^{-1} (Ni) for the $D = 23$ nm sample is only half the magnitude of 54 emu g^{-1} for bulk Ni. Following [34], this decrease in M_s can be interpreted in terms of a magnetically silent surface layer of Ni atoms as a result of the reduced symmetry and reduced exchange coupling of the surface spins to the spins in the bulk of an NP. Consequently, the surface spins are often disordered and so they do not contribute to M_s. For the Ni/SiO_2 system, this effect may be even more enhanced if there is likely some chemical coupling between the surface Ni atoms and the surrounding SiO_2 matrix, thus affecting the magnetism of the surface Ni atoms. However, the surface Ni atoms are not the likely source of line 3 since their effect would then have been more enhanced in the smaller 3.8 nm particles, similar to the large reduction in their magnetization seen in figure 15. This is so because the fraction of surface spins varies as $1/D$, thus increasing with decrease in D. Comparing the EMR profiles in figures 2–4 for different sizes, the intensity of line 3 certainly does not increase with decreasing D. Besides, the RS model [22] seems to provide an adequate description of the temperature dependence of line 2 and line 3 as discussed above.

7. Concluding remarks

Analysis of the experimental results on the temperature dependence of the three EMR lines observed in the nanocomposite Ni/SiO_2 (15/85) has been presented. Two of the lines (lines 2 and 3) are assigned to the Ni NPs and the third narrower line near $g = 2.00$ is attributed to paramagnetic defects in the amorphous SiO_2 matrix. Two models are used to interpret the temperature variation of H_r and ΔH for lines 2 and 3 assigned to Ni NPs. In the first model following Sharma

and Baiker [6], line 2 near $g = 2.2$ is assigned to the majority of the Ni NPs which, upon decreasing the temperature, go through a transition from the superparamagnetic to the blocked ferromagnetic state and line 3 near $g \approx 8$ is assigned to larger clusters of NPs which are in the blocked state even at 300 K. However, the large g value of line 3 and its dependence on particle size is difficult to explain in this model. In the second RS model based on the theory of Raikher and Stepanov [22], line 3 is a part of the inhomogeneously broadened asymmetric line 2 in the EMR absorption which appears as a separate line when the field derivative of absorption is measured in the experimental EMR spectra. Furthermore, the RS model predicts that, with increasing temperature, the composite line becomes more symmetric, its H_r increases and ΔH decreases in cubic systems with negative anisotropy such as Ni. The results presented here on Ni NPs provide strong support for these predictions. The RS model also predicts ΔH to reach a minimum at higher temperatures as observed here in the Ni NPs near 300 K. However, two additional predictions of the RS model remained untested. First, the RS model predicts increasing H_r with decreasing temperatures in a cubic system with positive anisotropy constant such as Fe NPs; and second ΔH is predicted to increase with increasing temperatures above the minimum near 300 K. In the work of Sharma and Baiker [6], a hint of increasing ΔH near 300 K was reported. However, we are not aware of any experimental work on the temperature dependence of the EMR parameter in Fe NPs to test the remaining prediction of the RS model.

In summary, the RS model provides a satisfactory explanation of the experimental results presented here on the Ni NPs. Verification of the other predictions of the RS model noted above will be undertaken in our future work. Establishing the SiO_2 matrix as the source of the narrow line whose linewidth and line position do not change with temperature is another important contribution of the results presented in this paper. Nanoparticles of Ni with high dispersion on a catalyst support such as SiO_2 and Al_2O_3 are excellent catalysts for various hydrogenation and hydrogenolysis reactions [3]. The method of synthesis and the corresponding properties of the Ni/SiO_2 nanocomposites with different dispersions of Ni presented here provide a good resource for future such applications.

Acknowledgment

Financial support provided by the US Department of Energy (contract no. DE-FC26-05NT42456) is gratefully acknowledged.

References

[1] Pankhurst Q A, Connolly J, Jones S K and Dobson J 2003 *J. Phys. D: Appl. Phys.* **36** R167
Gould P 2004 *Mater. Today* **7** 36
[2] Neuberger T, Schopf B, Hofmann H, Hoffman M and Rechenberg B V 2005 *J. Magn. Magn. Mater.* **293** 483
[3] Leite E R, Carreño N L V, Longo E, Valentini A and Probst L F D 2002 *J. Nanosci. Nanotech.* **2** 89
[4] Nikitin P I, Vetoshko P M and Ksenevich T I 2007 *J. Magn. Magn. Mater.* **311** 445
[5] Andreev A A and Selwood P W 1975 *J. Catal.* **8** 375
[6] Sharma V K and Baiker A 1981 *J. Chem. Phys.* **75** 5596
[7] Gittleman J I, Abeles B and Bozowski S 1974 *Phys. Rev.* B **9** 3891
[8] Sahoo Y, He Y, Swihart M T, Wang S, Luo H, Furlani E P and Prasad P N 2005 *J. Appl. Phys.* **98** 054308
[9] Zhang P, Zuo F, Urban F K III, Khabari A, Griffiths P and Tehrani A H 2001 *J. Magn. Mater.* **225** 337
[10] Fonseca F C, Goya G F, Jardim R F, Muccillo R, Carreño N L V, Longo E and Leite E R 2002 *Phys. Rev.* B **66** 104406
Fonseca F C, Goya G F, Jardim R F, Muccillo R, Carreño N L V, Longo E and Leite E R 2003 *J. Appl. Phys.* **93** 6531
[11] Singh V, Seehra M S and Bonevich J 2008 *J. Appl. Phys.* **103** 07D524
[12] Singh V, Seehra M S and Bonevich J 2009 *J. Appl. Phys.* **105** 07B518
[13] Singh V 2009 Size dependent magnetic properties of nickel nanoparticles embedded in silica matrix *PhD Dissertation* West Virginia University
[14] Berger R, Kliava J, Bissey J and Baietto V 1998 *J. Phys.: Condens. Matter* **10** 8559
Berger R, Kliava J, Bissey J and Baietto V 2000 *J. Appl. Phys.* **87** 7389
[15] Sharma V K and Baiker A J 1977 *J. Appl. Phys.* **48** 4298
[16] Usselman R J, Klen M T, Allen M, Walter E D, Gilmore K, Douglas T, Young M, Idzerda Y and Sviger D J 2005 *J. Appl. Phys.* **97** 10M523
[17] Noginova M, Chen F, Weaver T, Giannelis E P, Bourlinos A B and Atsarkin V A 2007 *J. Phys.: Condens. Matter* **19** 246208
[18] Devine R A B 1988 *The Physics and Technology of Amorphous SiO_2* (New York: Plenum)
Stirling A and Pasqualello A 2002 *Phys. Rev.* B **66** 245201
[19] Wohlfarth E P 1980 *Ferromagnetic Materials* vol 1 (New York: North-Holland) pp 1–70
[20] Morrish A H 2001 *The Physical Principles of Magnetism* (New York: Institute of Electrical and Electronic Engineers) p 562
[21] de Biasi R S and Devezas T C 1978 *J. Appl. Phys.* **49** 2466
[22] Raikher Y L and Stepanov V I 1992 *Sov. Phys.—JETP* **75** 764
[23] Castner T G and Seehra M S 1971 *Phys. Rev.* B **4** 38
[24] Huber D L and Seehra M S 1976 *Phys. Status Solidi* b **74** 145
[25] Kittel C 1996 *Introduction to Solid State Physics* 7th edn (New York: Wiley) p 449 and p 505
[26] Nagata K and Ishihara A 1992 *J. Magn. Magn. Mater.* **104–107** 1571
[27] Hsu K H, Wu J H, Huang Y Y, Wang L Y, Lee H Y and Lin J G 2005 *J. Appl. Phys.* **97** 114322
[28] Punnoose A, Seehra M S, Tol J V and Brunel L C 2005 *J. Magn. Magn. Mater.* **288** 168
[29] Seehra M S, Punnoose A, Roy P and Manivannan A 2001 *IEEE Trans. Magn.* **37** 2207
[30] Dutta P, Manivannan A, Seehra M S, Shah N and Huffman G P 2006 *J. Appl. Phys.* **99** 08H105
[31] Seehra M S, Dutta P, Shim H and Manivannan A 2004 *Solid State Commun.* **129** 721
[32] Morais P C, Lara M C L and Neto K S 1987 *Phil. Mag. Lett.* **55** 181
[33] Morais P C, Lara M C L and Tourinho F A 1996 *J. Magn. Reson.* A **121** 70
[34] Dutta P, Pal S, Seehra M S, Shah N and Huffman G P 2009 *J. Appl. Phys.* **105** 07B501